Monotone and Bounded Neural Operators in Conservative Drift-Flux Models for Soluble Methane Influx in Drilling

Pham Quoc Huy[1], Bui Thanh Nam[2], and Doan Minh Khoa[3]

[1]Vietnam Maritime University, Faculty of Electrical and Electronic Engineering, 484 Lach Tray Street, Le Chan District, Hai Phong 180000, Vietnam
[2]Hanoi University of Mining and Geology, Faculty of Information Technology, 18 Pho Vien Street, Duc Thang Ward, Bac Tu Liem District, Hanoi 100000, Vietnam
[3]Ho Chi Minh City University of Technology (HCMUT), Faculty of Engineering, 268 Ly Thuong Kiet Street, District 10, Ho Chi Minh City 700000, Vietnam

Abstract

Drilling annulus transients involving gas influx remain difficult to model and interpret because surface observables are shaped by compressibility, slip, temperature variation, and the partitioning of methane between free and dissolved inventories in synthetic or oil-based drilling fluids. While mechanistic models provide important physical structure, their operational use is often constrained by uncertain closure relations and by numerical fragility when regimes change rapidly. This paper develops a physics–machine-learning framework that targets a specific gap: learning closure operators for annular multiphase transport and dissolution while guaranteeing physical admissibility of the coupled simulator. The approach embeds monotone and bounded neural operators into a conservative drift-flux annular model with an explicit dissolved-gas inventory. Neural components represent uncertain mappings such as drift velocity, effective friction, swelling, and mass-transfer intensity, but are constructed to satisfy invariance constraints that enforce nonnegativity of phase masses, holdup bounds, and thermodynamic consistency of dissolution. Training uses a hybrid objective combining sparse surface measurements with weak physics residual penalties and inequality barrier terms that enforce admissibility across the training distribution and under extrapolation. A stability analysis shows how monotonicity and Lipschitz constraints on learned operators yield discrete-time invariance of the admissible state set under implicit time integration. Numerical experiments spanning circulating and near-static regimes demonstrate that the learned-closure simulator reduces bias in pressure and pit-gain predictions under closure uncertainty while avoiding unphysical states that can arise in unconstrained learning. The resulting model class is designed as a reliable computational kernel for real-time monitoring and uncertainty propagation in soluble kick environments.

1 Introduction

Transient gas influx into a drilling annulus is a coupled thermo-hydrodynamic process in which a downhole disturbance propagates through a spatially distributed multiphase system before it becomes observable at the surface [1]. The propagation is governed by compressibility, slip between phases, frictional pressure loss, heat exchange, and, in synthetic or oil-based drilling fluids, the dissolution and exsolution of methane that can store gas mass in the liquid and later release it as pressure decreases. These mechanisms yield a characteristic asymmetry: early signals can be weak and ambiguous because free-gas holdup may remain small, while later behavior can accelerate because exsolution and expansion amplify the surface response. Operationally, this creates the familiar tension between false alarms triggered by benign transients and missed detections when early influx is masked by solubility.

The modeling literature has approached this problem primarily through transient multiphase flow simulators coupled with varying levels of thermodynamic detail [2]. Yet the practical obstacles to operational deployment are not limited to model fidelity. They include closure uncertainty, numerical stiffness, and the fact that many inputs and parameters are poorly known at runtime. Drift velocity correlations for annular bubbly flow are uncertain across geometries and rheologies; effective friction in non-Newtonian drilling fluids is sensitive to temperature, shear, and cuttings; and solubility and swelling behavior depend on mud formulation and pressure-temperature history. These

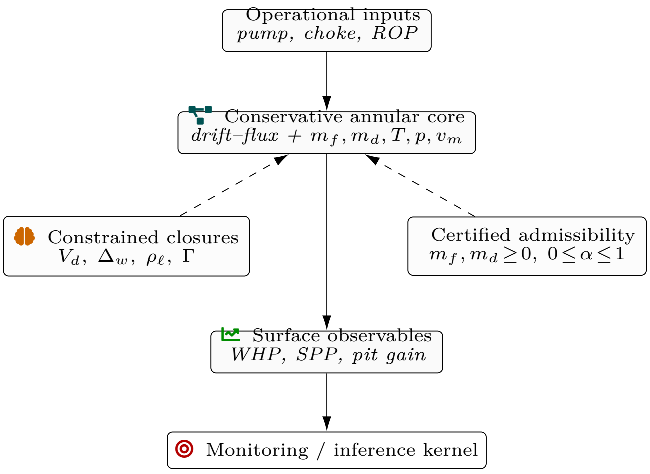

Figure 1: Physics–ML coupling used as a monitoring kernel: a conservative drift–flux annular model with explicit free and dissolved methane inventories is driven by operational inputs and augmented by constrained neural closure operators. The coupling is designed so that admissibility constraints (nonnegative inventories and bounded holdup) remain invariant while surface observables remain predictive under closure uncertainty.

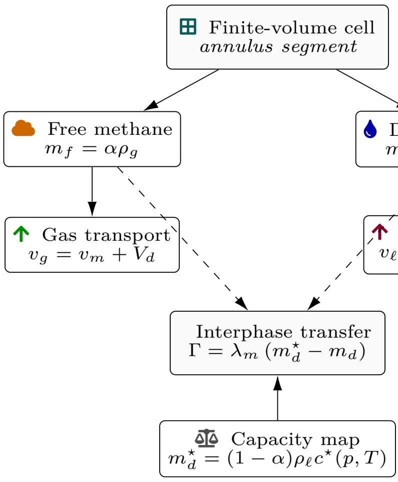

Figure 2: Inventory split inside a control volume: methane is tracked as free gas mass m_f and dissolved mass m_d, transported with drift–flux kinematics and coupled by a relaxation transfer rate Γ toward an equilibrium capacity $m_d^\star(p, T, \alpha)$. This explicit split exposes admissibility constraints and prevents ill-conditioning when holdup varies rapidly.

uncertainties matter because monitoring systems rely on the simulator not only for forward prediction but also as an implicit hypothesis class: when the simulator cannot represent the true physics within plausible parameter ranges, estimation and decision logic can be biased in ways that are difficult to detect from surface data alone [3]. A review of early gas-kick detection approaches notes that transient one-dimensional two-phase models dominate practice, often incorporating limited heat transfer and solubility and remaining constrained in operating conditions, while also emphasizing that dynamic multiphase modeling is central to early detection yet still limited by modeling scope and conditions [4]. This motivates a complementary emphasis: the model used in operational loops must be robust under uncertainty and must not fail physically or numerically in regimes that matter for safety.

Recent developments in physics-informed machine learning suggest that uncertain closures can be learned from data rather than specified purely by empirical correlations. However, unconstrained learning in multiphase systems can be unsafe in a literal sense: it can yield negative phase masses, holdup values outside $[0, 1]$, or nonphysical pressure responses that arise from a learned component violating monotonicity or boundedness. Such failures are not merely cosmetic [5]. They can produce large transient artifacts in pit gain and wellhead pressure that resemble kick signatures, or they can suppress true signatures by introducing spurious damping. Therefore, the key question is not whether a neural network can fit historical data, but whether one can learn closure operators while guaranteeing that the coupled simulator remains inside a physically admissible state set for all inputs and uncertainties encountered online.

This paper develops a closure-learning framework designed around certified admissibility. The central thesis is that, for soluble kick environments, a useful physics–ML model class must satisfy two requirements simultaneously:

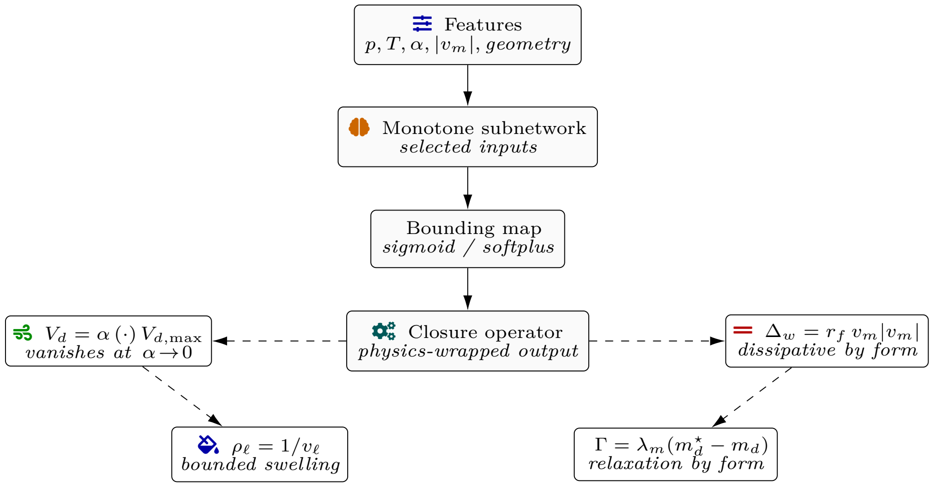

Figure 3: Constraint-preserving operator template: monotone subnetworks combined with explicit bounding transforms produce closure outputs that remain sign-consistent, bounded, and well-conditioned under extrapolation. Physics wrappers (e.g., α-factors and dissipative forms) encode limiting behavior and guarantee key inequalities needed for admissibility.

Symbol	Description	Units / notes
$p(z,t)$	Pressure in the annulus cell	Pa or MPa
$v_m(z,t)$	Mixture superficial velocity	m s^{-1}
$T(z,t)$	Mixture temperature	K or °C
$\alpha(z,t)$	Free-gas holdup (gas volume fraction)	Dimensionless, $0 \le \alpha \le 1$
$m_d(z,t)$	Dissolved methane mass per mixture volume	kg m^{-3}
$m_f(z,t)$	Free methane mass per mixture volume	kg m^{-3}

Table 1: Primary state variables used for soluble gas-kick transients in the annular drift-flux formulation.

it must be flexible enough to represent uncertain closure relations that vary across wells and conditions, and it must preserve the invariants of the underlying conservation laws and thermodynamic constraints [6]. The contribution is a family of monotone and bounded neural closure operators embedded in a conservative drift-flux annular model with explicit dissolved-gas inventory, along with a training and integration strategy that guarantees invariance of a physically admissible set under time stepping. Rather than treating the simulator as a black box, the approach treats the learned closures as constrained operators whose architecture is chosen so that key inequalities are preserved by construction.

The method is motivated by two practical observations. The first is that closure uncertainty is structured [7]. Drift velocity must be nonnegative in upward buoyant rise regimes and must vanish as holdup goes to zero; friction must dissipate momentum and cannot inject energy; solubility capacity must increase with pressure over relevant ranges and remain bounded; and mass transfer must move the dissolved concentration toward equilibrium rather than away from it. These requirements can be expressed as monotonicity, positivity, and Lipschitz constraints, which can be built into neural architectures using monotone networks and bounded activation functions. The second observation is that operational data are sparse and biased toward surface variables. Therefore, closure learning must exploit weak supervision: it must learn from pressure and pit-volume signals that are filtered through transport, while using the governing equations as constraints and using inequality barriers to prevent the model from using unphysical states as a shortcut to fit data.

The paper proceeds by first stating a conservative annular model with explicit free and dissolved methane inventories, chosen to expose the constraints that must be preserved [8]. A set of closure operators is then identified as the uncertainty locus, and each is represented by a constrained neural operator. A training formulation is developed that combines measurement mismatch with physics residual penalties and with admissibility barriers. A stability analysis shows that if the learned operators satisfy monotonicity and boundedness conditions, then a discrete-time integrator can be constructed that preserves nonnegativity and holdup bounds. Numerical experiments then demonstrate that the approach reduces prediction bias in surface signals under closure uncertainty while preventing unphysical states in regimes where unconstrained learning commonly fails [9].

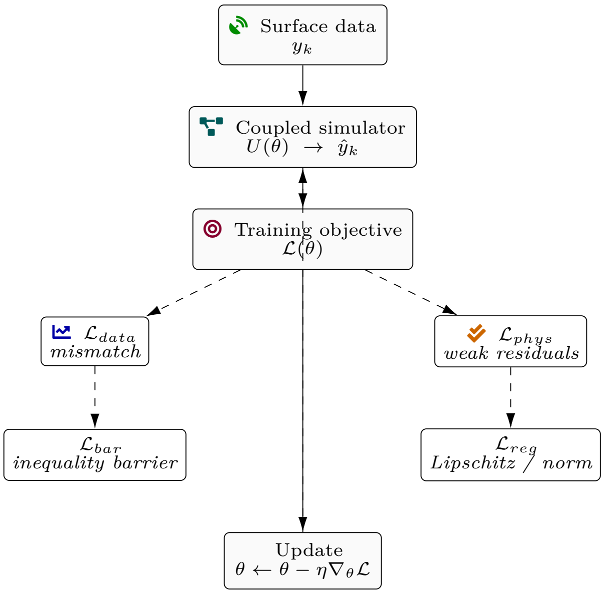

Figure 4: Weakly supervised closure learning: surface measurements supervise the coupled simulator through a composite objective that combines data mismatch, soft physics consistency, admissibility barriers, and sensitivity regularization. The loop updates closure parameters while maintaining physically meaningful trajectories during optimization and extrapolation.

Quantity	Definition	Comment
m_d	$m_d = (1-\alpha)\,\rho_\ell(p, T, m_d)\,c$	Dissolved methane mass per mixture volume
m_f	$m_f = \alpha\,\rho_g(p, T)$	Free methane mass per mixture volume
m_g	$m_g = m_f + m_d$	Total methane mass per mixture volume
ρ_m	$\rho_m = \alpha\rho_g + (1-\alpha)\rho_\ell$	Mixture density entering conservation laws

Table 2: Definitions of methane inventory variables and mixture density entering the conservative formulation.

2 Annular Dynamics with Explicit Dissolved Inventory and Closure Uncertainty

Consider an annulus or riser of length L parameterized by measured depth $z \in [0, L]$, with $z = 0$ at the surface. The annulus has cross-sectional area $A(z)$, hydraulic diameter $D_h(z)$, and inclination $\theta(z)$. The mixture consists of a liquid drilling fluid and methane that may exist as free gas and as dissolved gas in the liquid. The state variables are pressure $p(z,t)$, mixture superficial velocity $v_m(z,t)$, temperature $T(z,t)$, free-gas holdup $\alpha(z,t)$, and a dissolved methane inventory variable chosen to avoid ill-conditioning when α approaches one [10]. To that end, define dissolved methane mass per mixture volume $m_d(z,t) = (1-\alpha)\rho_\ell(p, T, m_d)\,c(z,t)$, where ρ_ℓ is liquid density and c is dissolved methane concentration per unit liquid mass. Define free methane mass per mixture volume $m_f(z,t) = \alpha\rho_g(p,T)$, where ρ_g is methane density. Total methane mass per mixture volume is $m_g = m_f + m_d$.

The governing equations are written in conservative form for mixture mass, methane inventories, and mixture momentum, with a reduced energy balance to couple temperature to density and solubility capacity. Mixture density is $\rho_m = \alpha\rho_g + (1-\alpha)\rho_\ell$, and mixture mass conservation is [11]

$$\frac{\partial}{\partial t}(A\rho_m) + \frac{\partial}{\partial z}(A\rho_m v_m) = 0. \tag{1}$$

Methane inventories evolve through transport and interphase mass transfer. Using drift-flux kinematics, the gas

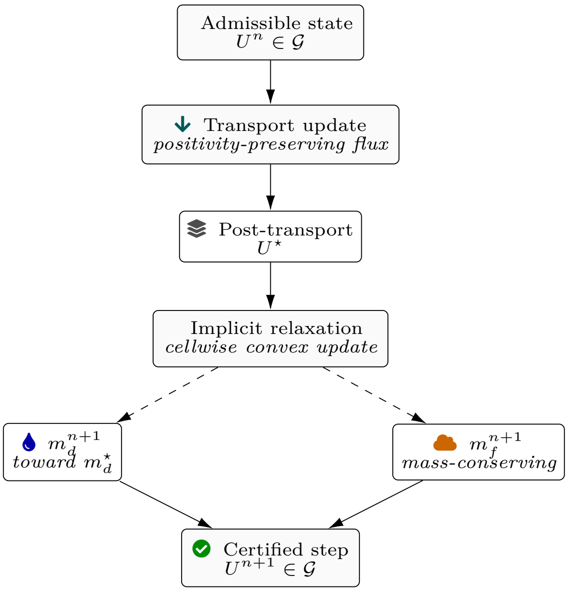

Figure 5: Discrete admissibility mechanism: an operator-split step combines a positivity-preserving transport update with an implicit relaxation update for mass transfer. The relaxation is structured as a convex cellwise update that preserves nonnegativity of inventories while conserving total methane, enabling certified invariance of the admissible set under time stepping.

Closure	Physical role	Main dependencies	Admissibility constraints
V_d	Drift velocity between gas and liquid	α, p, T, v_m, geometry	$0 \le V_d \le V_{d,\max}$, $V_d \to 0$ as $\alpha \to 0$
Δ_w	Wall shear (friction)	v_m, ρ_m, rheology	$\Delta_w v_m \ge 0$ (dissipative)
ρ_ℓ	Liquid density with swelling	p, T, m_d	$\rho_{\ell,\min} \le \rho_\ell \le \rho_{\ell,\max}$, $\partial\rho_\ell/\partial m_d \le 0$
$m_d^\star$	Equilibrium dissolved mass	p, T, α	Monotone in p, bounded, consistent with $0 \le \alpha \le 1$
Γ	Interphase mass transfer	$m_d, m_d^\star, \xi_m$	$\Gamma(m_d - m_d^\star) \le 0$, $\Gamma = 0$ at equilibrium

Table 3: Uncertain closure operators in the annular model and representative admissibility constraints imposed on each mapping.

and liquid velocities are

$$v_g = v_m + V_d(\alpha, p, T, v_m; \eta), \quad v_\ell = v_m - \frac{\alpha}{1-\alpha} V_d(\alpha, p, T, v_m; \eta), \tag{2}$$

where V_d is a drift velocity and η denotes closure parameters. The methane inventory balances are [12]

$$\frac{\partial}{\partial t}(A m_f) + \frac{\partial}{\partial z}(A m_f v_g) = -A\Gamma + A s_{in}, \tag{3}$$

$$\frac{\partial}{\partial t}(A m_d) + \frac{\partial}{\partial z}(A m_d v_\ell) = A\Gamma, \tag{4}$$

where $\Gamma(z,t)$ is the interphase transfer rate per mixture volume, positive for dissolution and negative for exsolution, and s_{in} represents gas entry from the formation, typically as a boundary influx near $z = L$. Mixture momentum is modeled as

$$\frac{\partial}{\partial t}(A\rho_m v_m) + \frac{\partial}{\partial z}\left(A\rho_m v_m^2\right) + A\frac{\partial p}{\partial z} = -A\rho_m g \cos\theta - A\Delta_w, \tag{5}$$

where Δ_w is wall shear per mixture volume, which is dissipative. A reduced thermal evolution is included through a mixture temperature balance

$$\frac{\partial}{\partial t}(A\rho_m h_m) + \frac{\partial}{\partial z}(A\rho_m v_m h_m) = -A v_m \frac{\partial p}{\partial z} + A q_{\text{wall}}(T, T_f; \kappa), \tag{6}$$

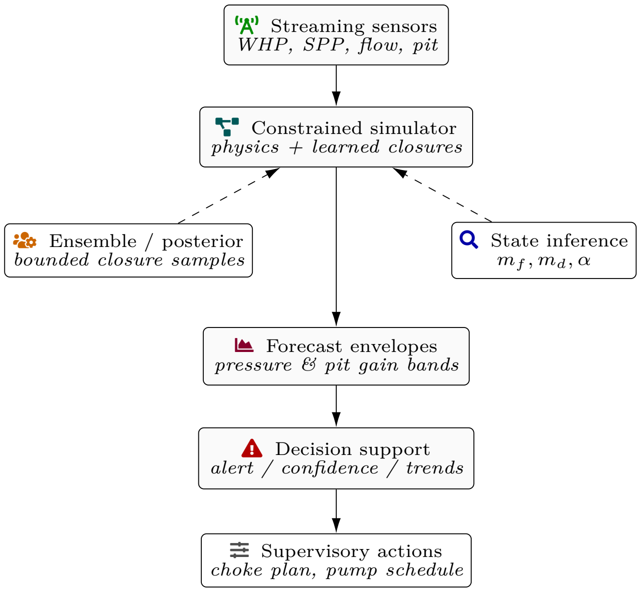

Figure 6: Operational deployment concept: streaming surface data drive a constrained, closure-adaptive annular simulator used for state inference and ensemble uncertainty propagation. The output is a set of physically admissible forecast envelopes that support conservative decision logic during soluble gas-kick transients where early signals may be masked by dissolution.

where h_m is mixture enthalpy, $T_f(z)$ is an ambient profile, and κ is an effective heat transfer parameter [13]. In the learning framework, the thermal equation is used primarily to produce consistent temperature dependence in ρ_g, ρ_ℓ, and solubility capacity, rather than to resolve fine thermal features.

The closure uncertainty is concentrated in four mappings. The drift velocity V_d determines migration timing. The friction term Δ_w determines pressure response to circulation and holdup. The liquid property response to dissolved methane, represented through $\rho_\ell(p, T, m_d)$, determines swelling and hydrostatic feedback [14]. The interphase mass transfer Γ determines how quickly methane partitions between free and dissolved inventories. Each mapping depends on variables that vary across wells and operations and is therefore an appropriate target for learning.

The drift velocity must satisfy constraints consistent with the limiting behavior of bubbly flow in an annulus. It should be nonnegative for upward buoyant slip in near-vertical segments, should vanish as $\alpha \to 0$, and should remain bounded to prevent unphysical gas velocities [15]. A generic constraint set can be expressed as

$$0 \le V_d(\alpha, p, T, v_m) \le V_{d,\max}(p, T, v_m), \quad \lim_{\alpha \to 0} V_d(\alpha, p, T, v_m) = 0. \tag{7}$$

The friction term must dissipate momentum. A sufficient constraint is that the friction force is opposite to velocity:

$$\Delta_w(\cdot)\, v_m \ge 0 \quad \text{for all admissible states.} \tag{8}$$

The swelling response must preserve positivity of liquid density and bounded compressibility [16]. A practical constraint is

$$\rho_{\ell,\min}(p, T) \le \rho_\ell(p, T, m_d) \le \rho_{\ell,\max}(p, T), \quad \frac{\partial \rho_\ell}{\partial m_d} \le 0 \text{ and bounded in magnitude.} \tag{9}$$

Mass transfer must relax toward equilibrium rather than away from it. Let $m_d^\star(p, T, \alpha)$ denote the equilibrium dissolved methane mass per mixture volume. A standard relaxation form is

$$\Gamma = k_m a_i \big(m_d^\star(p, T, \alpha; \chi) - m_d\big), \quad k_m a_i \ge 0, \tag{10}$$

where k_m is a mass-transfer coefficient, a_i is interfacial area density, and χ parameterizes solubility capacity [17]. The required property is monotone dissipation:

$$\Gamma\,(m_d - m_d^\star) \le 0, \quad \Gamma = 0 \text{ iff } m_d = m_d^\star \text{ or } a_i = 0. \tag{11}$$

The equilibrium map $m_d^\star$ must itself be monotone in pressure in the relevant range, bounded, and consistent with $0 \le \alpha \le 1$ through the $(1-\alpha)$ factor implicit in dissolved capacity.

Mechanistic modeling of these phenomena has been advanced in compact annular simulators. Manikonda et al. (2019) [18] developed a cutting-edge semi-analytical model for gas kick behavior in annuli that explicitly

Mapping	Neural construction	Guaranteed property
V_d	$V_d = \alpha\,\sigma_d(\alpha)\,V_{d,\max}\,\phi_d(\xi_d)$ with $\phi_d \in [0,1]$	Bounded, non-negative drift, $V_d \to 0$ as $\alpha \to 0$
Δ_w	$\Delta_w = r_f(\xi_f)\,v_m\,\lvert v_m\rvert$ with $r_f \geq 0$ (softplus)	Always dissipates momentum, no energy injection
ρ_ℓ	$v_\ell = v_{\ell,0}(1 + s_\ell \psi_\ell)$, $\psi_\ell \in [0,1]$, monotone in m_d	Positive, bounded density with $\partial\rho_\ell/\partial m_d \leq 0$
$c^\star$	$c^\star = c_{\min} + (c_{\max} - c_{\min})\,\sigma(u_s)$, monotone in p	Bounded, pressure-increasing solubility capacity
Γ	$\Gamma = \lambda_m(\xi_m)\,(m_d^\star - m_d)$ with $\lambda_m \geq 0$	Relaxation toward equilibrium without overshoot

Table 4: Neural parameterizations of closure operators chosen to enforce monotonicity, boundedness, and sign constraints by design.

Quantity	Inequality	Interpretation	Consequence
$\rho_{m,i}$	$\rho_{m,i} > 0$	Positive mixture mass density	Prevents vacuum or sign flips
$m_{f,i}$	$m_{f,i} \geq 0$	Nonnegative free methane mass	Avoids unphysical negative gas inventory
$m_{d,i}$	$m_{d,i} \geq 0$	Nonnegative dissolved methane mass	Ensures physical dissolution state
α_i	$0 \leq \alpha_i \leq 1$	Holdup within volume-fraction bounds	Keeps mixture composition admissible
T_i	$T_i > 0$	Positive absolute temperature	Prevents breakdown of EOS and solubility

Table 5: Representative inequalities defining the admissible discrete state set $\mathcal{G}$ for the finite-volume annular model.

incorporated gas solubility in oil-based drilling fluids and showed that solubility can delay wellhead arrival relative to insoluble assumptions, reinforcing that dissolved inventory is not a secondary correction but a mechanism that changes surface indicator timelines [19]. In the present paper, this motivates the modeling choice to treat m_d as a primary state and to treat $m_d^\star$ and Γ as central closures whose constraints must be preserved in learning.

The model is discretized in space using a finite-volume method to obtain a finite-dimensional dynamical system. Let $i = 1, \ldots, N$ index cells and let U_i denote a vector of conservative quantities in cell i. The discrete update is written as [20]

$$U_i^{n+1} = U_i^n - \frac{\Delta t}{V_i}\left(\widehat{F}^n_{i+\frac{1}{2}} - \widehat{F}^n_{i-\frac{1}{2}}\right) + \Delta t\, S_i^{n+\frac{1}{2}}, \tag{12}$$

where $\widehat{F}$ are numerical fluxes and S includes friction, gravity, heat exchange, and mass transfer. The admissible set $\mathcal{G}$ of physically meaningful discrete states is defined by nonnegativity of mixture mass and methane inventories and by holdup bounds. In discrete variables, a representative admissible set is

$$\mathcal{G} = \{U : \rho_{m,i} > 0,\ m_{f,i} \geq 0,\ m_{d,i} \geq 0,\ 0 \leq \alpha_i \leq 1,\ T_i > 0 \text{ for all } i\}. \tag{13}$$

The central goal of the paper is to learn the uncertain closures while guaranteeing that the time-stepped dynamics map $\mathcal{G}$ into itself for all admissible inputs and disturbances.

Term	Expression	Role in training
$\mathcal{L}_{\text{data}}$	$\sum_k (y_k - \hat{y}_k)^\mathsf{T} W (y_k - \hat{y}_k)$	Match surface pressure and pit-volume measurements
$\mathcal{L}_{\text{phys}}$	$\sum_{n,i} \lVert R_i^n \rVert^2$	Penalize violation of discrete mass and energy balances
$\mathcal{L}_{\text{bar}}$	$\sum_{n,i,j} \varphi(g_j(U_i^n))$	Act as barrier near boundaries of $\mathcal{G}$
$\mathcal{L}_{\text{reg}}$	Weight decay and Lipschitz penalties on networks	Control complexity and sensitivity of closures

Table 6: Components of the composite loss functional used to train constraint-preserving neural closures from sparse operational data.

Aspect	Unconstrained learning	Constraint-preserving learning	Impact on operation
Drift velocity	Possible negative or unbounded V_d in extrapolation	V_d monotone, bounded, $V_d \to 0$ as $\alpha \to 0$	Robust migration timing without spurious reversal
Friction term	Network can predict $\Delta_w v_m < 0$	$\Delta_w = r_f v_m \lvert v_m \rvert$, always dissipative	Avoids self-excited pressure oscillations
Solubility map	$c^\star(p,T)$ can be non-monotone or unbounded	Bounded, pressure-increasing $c^\star$	Consistent dissolved inventory evolution
Mass transfer	Arbitrary sign changes in Γ	Relaxation $\Gamma = \lambda_m(m_d^\star - m_d)$	No artificial source/sink of methane mass
Numerical stability	Frequent solver failures in stiff regimes	Positivity-preserving, CFL-controllable scheme	Stable simulation across regimes
Uncertainty envelopes	Outlier trajectories from extreme closures	Bounded ensembles respecting admissibility	Meaningful probabilistic envelopes for monitoring

Table 7: Qualitative comparison between unconstrained neural closures and the proposed constraint-preserving operators in terms of behavior and operational consequences.

3 Constraint-Preserving Neural Closure Operators

The closures V_d, Δ_w, ρ_ℓ, and Γ are represented by neural operators designed to satisfy physical constraints by construction. The key design choice is to avoid generic multilayer perceptrons that can produce arbitrary signs and unbounded outputs. Instead, each learned mapping is built from monotone subnetworks, bounded transforms, and explicit multiplicative factors that impose limiting behavior at $\alpha \to 0$ and $(1-\alpha) \to 0$.

The drift velocity is represented as a product of a vanishing holdup factor and a bounded positive function of state [21]. Let ϕ_d be a neural network with nonnegative output. Define

$$V_d(\alpha, p, T, v_m) = \alpha\, \sigma_d(\alpha)\, V_{d,\max}(p, T, v_m)\, \phi_d(\xi_d), \quad 0 \le \phi_d(\cdot) \le 1, \tag{14}$$

where $\sigma_d(\alpha)$ is a smooth hindrance factor bounded in $[0,1]$, $V_{d,\max}$ is a physics-based bound such as a buoyancy scaling, and ξ_d is a feature vector including normalized p, T, $|v_m|$, and geometry descriptors. The factor α ensures $V_d \to 0$ as $\alpha \to 0$, while the bounded ϕ_d and $V_{d,\max}$ ensure V_d remains bounded. The network ϕ_d is implemented using a sigmoid output to enforce $[0,1]$. If monotonicity in certain inputs is desired, such as increasing drift with hydraulic diameter or decreasing drift with viscosity, the internal network is chosen as a monotone neural network with nonnegative weights on selected features, implemented via weight-positivity constraints and monotone activations [22].

The friction closure is constructed to guarantee dissipation. Rather than predicting Δ_w directly, the network

Regime	Dominant mechanisms	Observed behavior
Circulating	Friction, drift, and heat exchange	Pressure response to pump ramps, holdup redistribution
Near-static	Buoyancy, dissolution, residual circulation	Slow migration, weak early surface signals
Early soluble influx	High $c^\star$, strong dissolution capacity	Free gas masked, small changes in wellhead pressure
Late exsolution-dominated	Falling pressure, shrinking $m_d^\star$	Rapid growth of m_f, accelerated pit gain and pressure changes
High-uncertainty operation	Poorly known friction and solubility	Wide but bounded envelopes for pressure and pit gain

Table 8: Representative operating regimes considered in the numerical experiments and the associated dominant physics under soluble kick conditions.

predicts a nonnegative friction magnitude r_f, and the friction term is defined as

$$\Delta_w = r_f(\xi_f)\, v_m\, |v_m|, \quad r_f(\xi_f) \geq 0, \tag{15}$$

so that $\Delta_w v_m = r_f v_m^2 |v_m| \geq 0$. The feature vector ξ_f includes Reynolds-like quantities, temperature, holdup, and shear-rate proxies [23]. Nonnegativity is enforced by representing r_f as a softplus of a neural output. Boundedness can be enforced by capping r_f with a smooth saturating transform. This prevents the learned friction from growing without bound in regimes where data are sparse, which would otherwise cause excessive stiffness and numerical instability.

Liquid density response to dissolved methane is represented by a bounded swelling map in specific volume rather than density directly. Let v_ℓ be liquid specific volume [24]. Define

$$v_\ell(p, T, m_d) = v_{\ell,0}(p, T)\left(1 + s_\ell(p, T)\, \psi_\ell(\xi_\ell)\right), \quad \rho_\ell = \frac{1}{v_\ell}, \tag{16}$$

where $v_{\ell,0}(p, T)$ is a baseline specific volume, $s_\ell(p, T)$ is a bounded swelling scale, and $\psi_\ell(\cdot) \in [0, 1]$ is a bounded neural output. The bounded factor ensures that v_ℓ remains within $[v_{\ell,0}, v_{\ell,0}(1 + s_\ell)]$ and thus ρ_ℓ remains positive and bounded. To enforce that dissolved methane does not increase density, the neural network is constructed so that ψ_ℓ is nondecreasing in m_d by using a monotone architecture in the m_d input. This yields $\partial v_\ell/\partial m_d \geq 0$ and $\partial \rho_\ell/\partial m_d \leq 0$ as required.

The solubility equilibrium and mass transfer are represented in a way that guarantees relaxation [25]. The equilibrium dissolved mass $m_d^\star$ is written as

$$m_d^\star(p, T, \alpha) = (1 - \alpha)\, \rho_\ell(p, T, m_d)\, c^\star(p, T), \tag{17}$$

with $c^\star$ modeled as a bounded monotone map of (p, T). A convenient representation uses an unconstrained scalar output u_s mapped through a logistic function to keep $c^\star$ within physically meaningful bounds:

$$c^\star(p, T) = c_{\min}(T) + \left(c_{\max}(T) - c_{\min}(T)\right) \sigma(u_s(\xi_s)), \tag{18}$$

where $c_{\min}(T) \geq 0$ and $c_{\max}(T)$ are physically chosen envelopes and σ is a sigmoid. Monotonicity in pressure is enforced by choosing u_s as a monotone neural network in p with nonnegative weights on the pressure feature [26]. Temperature dependence can be left flexible within bounds, or monotone decreasing in T can be enforced similarly if desired.

Mass transfer is then defined as

$$\Gamma = \lambda_m(\xi_m)\left(m_d^\star(p, T, \alpha) - m_d\right), \quad \lambda_m(\xi_m) \geq 0, \tag{19}$$

Step	Description	Positivity mechanism
Transport update	Finite-volume update of U_i^n using numerical fluxes $\widehat{F}^n_{i\pm1/2}$	Monotone flux and CFL restriction preserve nonnegativity
Momentum / friction	Update of mixture momentum with gravity and Δ_w	Dissipative Δ_w prevents kinetic-energy growth
Mass transfer	Implicit relaxation of m_d, m_f toward $m_d^\star$	Convex combination keeps $m_f, m_d \geq 0$ and conserves m_g
Holdup correction	Local adjustment if $m_f > \rho_g(p, T)$	Repartitioning into dissolved phase while conserving methane
Time-step control	Selection of Δt from bounded characteristic speeds	Ensures discrete mapping keeps U_i^n inside $\mathcal{G}$

Table 9: Discrete-time update structure of the simulator and mechanisms used to maintain invariance of the admissible set under time stepping.

with λ_m representing the effective relaxation rate $k_m a_i$. Nonnegativity of λ_m is enforced by softplus, and boundedness is enforced by a saturating transform. Importantly, this construction enforces $\Gamma(m_d - m_d^\star) \leq 0$ automatically, guaranteeing relaxation toward equilibrium [27]. It also enables the model to represent circulation-dependent kinetics because ξ_m includes $|v_m|$ and shear proxies.

The key benefit of these constructions is that the learned closures are not free functions. They are constrained operators that preserve sign and boundedness properties needed for invariance and stability. This is essential for extrapolation, because operational conditions can move outside the convex hull of training data [28]. In unconstrained learning, extrapolation often produces unbounded outputs or sign flips. In the present framework, extrapolation changes the magnitude of bounded functions but cannot violate invariants.

Solubility models have been validated in mechanistic kick simulators that combine thermodynamic calculations with annular transport. Manikonda et al. (2020) proposed a mechanistic model for gas behavior in a riser with synthetic-based drilling fluids [29], explicitly modeling methane dissolution and comparing its solubility predictions against an external thermodynamic simulator while also reporting experimental observations in a laboratory flow loop. The narrative relevance here is that methane dissolution in synthetic oil-based drilling fluids can be represented with compact mechanistic structure; the present paper uses this as motivation to enforce thermodynamic consistency and bounded relaxation structure in the learned solubility operators rather than treating dissolution as an unstructured delay [30].

4 Training, Uncertainty Regularization, and Discrete Admissibility Guarantees

The closure operators are learned from data by minimizing a loss functional that combines measurement mismatch, physics consistency penalties, and inequality barriers enforcing admissibility. The training data consist of time series of surface measurements and operational inputs. Typical measured signals include wellhead pressure, standpipe pressure, pump rate, choke setting, and pit-volume change or return flow proxies. The model is simulated forward given inputs, and the closures are adjusted to reduce mismatch [31]. Because downhole states are unobserved, training is a weakly supervised inverse problem, and thus regularization and constraints are central.

Let θ denote the parameters of the neural closures. Let y_k denote measurements at discrete times t_k, and let $\hat{y}_k(\theta)$ denote predicted measurements computed by simulating the coupled PDE discretization. The primary data misfit term is

$$\mathcal{L}_{data}(\theta) = \sum_k \big(y_k - \hat{y}_k(\theta)\big)^\mathsf{T} W \big(y_k - \hat{y}_k(\theta)\big), \tag{20}$$

where W is a weighting matrix reflecting measurement noise [32]. To reduce the tendency to fit noise and to compensate for missing physics by distorting closures, physics residual penalties are added. For example, one may penalize deviations from mixture mass conservation and from energy balance beyond numerical truncation. In a finite-volume scheme, these residuals can be measured as imbalance terms. A generic residual penalty is

$$\mathcal{L}_{phys}(\theta) = \sum_{n,i} \|R_i^n(\theta)\|^2, \tag{21}$$

where R_i^n is a discrete residual at cell i and time step n [33]. This does not enforce exact PDE satisfaction, because numerical dissipation and modeling residuals exist, but it discourages closures that create systematic imbalances.

The central addition is an admissibility barrier that penalizes trajectories that approach or cross the boundary of the admissible set. Let $\mathcal{G}$ be defined by inequalities $g_j(U) \geq 0$. A smooth barrier term is

$$\mathcal{L}_{bar}(\theta) = \sum_{n,i} \sum_{j} \varphi(g_j(U_i^n(\theta))) \,, \tag{22}$$

where φ is large when g_j is near zero or negative, such as a log barrier on positive constraints [34]. The constraints include $m_{f,i} \geq 0$, $m_{d,i} \geq 0$, $\rho_{m,i} \geq \rho_{\min}$, and $0 \leq \alpha_i \leq 1$ expressed as $m_{f,i} \leq \rho_g(p_i, T_i)$. Because the closures are constructed to satisfy many constraints inherently, the barrier primarily guards against numerical errors and against constraint violations that can occur due to boundary conditions or extreme extrapolation.

The combined training objective is

$$\min_{\theta} \quad \mathcal{L}(\theta) = \mathcal{L}_{data}(\theta) + \lambda_{phys}\mathcal{L}_{phys}(\theta) + \lambda_{bar}\mathcal{L}_{bar}(\theta) + \lambda_{reg}\mathcal{L}_{reg}(\theta), \tag{23}$$

where $\mathcal{L}_{reg}$ includes weight decay and Lipschitz regularization. Lipschitz regularization is particularly important because it bounds the sensitivity of closures to inputs, which in turn affects stability of time stepping and robustness of inference. A practical Lipschitz bound is enforced by spectral normalization of network weights, ensuring that each neural operator has a known Lipschitz constant [35]. For monotone networks, weight nonnegativity constraints are combined with spectral normalization to control growth.

Training on long trajectories is computationally demanding. The framework uses implicit time stepping for stiff terms such as mass transfer and uses adjoint or truncated backpropagation through time to compute gradients. The training is performed on multiple operating regimes to reduce overfitting, including non-circulating and circulating conditions, because closures such as k_m and V_d can depend strongly on circulation.

The learning framework also incorporates uncertainty [36]. Because data are sparse, multiple parameter settings can fit the same measurements. Rather than producing a single best-fit closure, the framework can represent a posterior over θ via ensemble training or variational inference. However, the essential constraint is that every sampled closure must satisfy the admissibility constraints. This motivates using parameterizations where constraints hold for all θ, as in the bounded constructions above [37]. Uncertainty then manifests as variation within bounded ranges rather than as occasional constraint-violating samples.

A key analytical component is a discrete admissibility guarantee. The goal is to show that, under the constrained closure operators and under a suitable time-stepping scheme, the simulation map preserves $\mathcal{G}$. Consider an operator-split scheme in which transport is updated explicitly or semi-implicitly with a positivity-preserving flux, while mass transfer is updated implicitly by a convex combination. The mass-transfer update in each cell can be written as [38]

$$m_d^{n+1} = \frac{m_d^\star + \Delta t\, \lambda_m\, m_d^{\star\star}}{1 + \Delta t\, \lambda_m}, \quad m_f^{n+1} = m_f^\star + (m_d^\star - m_d^{n+1}), \tag{24}$$

where $m_d^\star$ and $m_f^\star$ are post-transport values, $m_d^{\star\star}$ is equilibrium capacity, and $\lambda_m \geq 0$. Because m_d^{n+1} is a convex combination of $m_d^\star$ and $m_d^{\star\star}$, it remains nonnegative if those are nonnegative. The equilibrium capacity is nonnegative by construction of $c^\star$. Free methane mass remains nonnegative if $m_d^{n+1} \leq m_f^\star + m_d^\star$, which is enforced by limiting $m_d^{\star\star}$ to available methane. Therefore, the mass transfer update preserves $m_f \geq 0$ and $m_d \geq 0$ unconditionally.

Transport updates preserve positivity under a CFL-like condition when using monotone fluxes. The drift velocity and friction closures influence characteristic speeds and thus the CFL bound. Because V_d is bounded by construction, and because friction does not alter transport CFL directly, the time step can be selected to satisfy a computable bound [39]. The result is that there exists a time step restriction such that the full split update maps $\mathcal{G}$ into itself.

Holdup bounds require additional care. Since $\alpha = m_f/\rho_g(p,T)$, ensuring $m_f \leq \rho_g$ is sufficient for $\alpha \leq 1$. Because m_f is transported and updated by mass transfer, enforcing $m_f \leq \rho_g$ is equivalent to enforcing that the free methane mass per volume does not exceed the maximum possible gas mass per volume, which is the gas density at that pressure and temperature. In the discrete update, m_f can temporarily exceed this bound if pressure is updated inconsistently [40]. The constrained closures mitigate this by keeping solubility and swelling bounded so that pressure does not jump unexpectedly, and the time-stepping scheme can enforce the bound by a local correction that adjusts m_f and m_d while conserving total methane and moving methane into the dissolved inventory when capacity allows. Because $m_d^\star$ includes $(1-\alpha)$ dependence, this correction is well defined in the physically relevant range. The correction can be interpreted as a local instantaneous equilibration step applied only when needed, which is consistent with the fact that the continuum representation is not reliable when α is extremely close to one.

The admissibility guarantee is important not only for stable forward simulation but also for training stability [41]. Without admissibility constraints, gradients can become undefined when states go negative or when logs of negative quantities appear in loss functions. By ensuring that trajectories remain in $\mathcal{G}$, training remains stable and optimization does not exploit unphysical regions.

5 Numerical Evaluation and Operational Interpretation Under Soluble Conditions

Numerical experiments illustrate the behavior of the constraint-preserving closure-learning framework and highlight its operational implications. The purpose is to assess two questions. The first is whether learned closures improve prediction of surface observables under uncertain drift, friction, and solubility without sacrificing physical admissibility. The second is whether the learned model behaves robustly across regimes, particularly in early ambiguous stages where dissolution masks free gas and in later stages where exsolution can accelerate changes [42].

The evaluation uses a set of synthetic and semi-synthetic scenarios generated from a high-fidelity reference model with known closures and then perturbed by uncertainty. Surface measurements are sampled with noise and bias typical of operational sensing, including drift in pit-volume measurement. The learning model is initialized with broad prior closure envelopes and is trained to match measured wellhead pressure and pit gain trajectories under known pump and choke inputs. The key comparison is between constrained learning and unconstrained learning [43]. In unconstrained learning, generic networks are used for closures without monotonicity or boundedness constraints. In constrained learning, the operators described earlier are used.

In circulating regimes, friction and drift uncertainties dominate pressure response. The constrained learning model learns an effective friction magnitude r_f that varies smoothly with Reynolds-like features and holdup, improving prediction of standpipe and wellhead pressure changes during pump ramps [44]. Because r_f is constrained to be nonnegative, it cannot inject momentum, and pressure predictions do not exhibit self-excited oscillations that sometimes appear in unconstrained models due to sign errors. The drift velocity operator learns a dependence on flow regime proxies that improves predicted migration timing, but it remains bounded and vanishes at small holdup, preventing spurious gas migration when no gas is present. In unconstrained learning, the drift velocity can become negative in some regimes, implying downward slip that conflicts with buoyancy in vertical wells and producing nonphysical delay or acceleration artifacts.

In non-circulating regimes, dissolution dominates early behavior when solubility capacity is high. The constrained solubility operator produces an equilibrium map $c^\star(p,T)$ that increases with pressure and remains bounded [45]. The mass transfer operator produces relaxation toward $m_d^\star$ without overshoot. As a result, early free methane mass remains small, and the predicted wellhead pressure remains close to baseline, consistent with the masking effect of dissolution. The key difference between constrained and unconstrained learning is not that constrained learning makes early signals larger. It is that constrained learning avoids using unphysical states to explain noise [46]. In unconstrained learning, the model can fit small pressure anomalies by creating negative dissolved inventory in some cells or by producing density increases with dissolved methane, which can change hydrostatic head in an unphysical direction. These pathologies can yield short-term fits but lead to later divergence when exsolution occurs, because the model has built an incorrect internal state.

In regimes where exsolution occurs, the constraints become even more important. As pressure decreases in upper sections, the equilibrium capacity drops, and dissolved methane must exsolve if total methane exceeds capacity [47]. The constrained model represents this as negative Γ driving m_d downward toward $m_d^\star$, producing m_f growth. Because the update is monotone and mass-conserving, exsolution produces a predictable increase in free methane mass without oscillation. In unconstrained learning, the exsolution response can chatter because the learned $c^\star$ map can be non-monotone in pressure, causing alternating dissolution and exsolution in adjacent time steps, which is a numerical artifact that can manifest as oscillatory pit gain. The bounded interfacial area surrogate in the constrained model also prevents exsolution kinetics from becoming arbitrarily fast due to learned spikes, which would force extremely small time steps or cause solver instability.

The evaluation also considers uncertainty propagation [48]. Because closures are learned with bounded outputs, ensembles of closures produce bounded variability in predicted pressure and pit gain. This is operationally useful because it supports conservative envelopes rather than single trajectories. In early stages of soluble events, uncertainty bands remain wide because surface observables are weakly informative. Later, when exsolution amplifies signals, the bands shrink because measurements constrain the internal methane inventory more strongly [49]. This behavior reflects physics-driven observability rather than overfitting. In unconstrained ensembles, some closure samples produce extreme outliers because of unbounded extrapolation, rendering ensemble envelopes unusable. The constrained design prevents such outliers.

An important operational interpretation is that the constrained learning model does not claim to eliminate early ambiguity [50]. Dissolution can genuinely mask early free gas, and no learning method can create information that measurements do not contain. Instead, the constrained model aims to provide reliable internal states and reliable envelopes under ambiguity, avoiding the false certainty that can arise when a model fits data by violating physics. This is particularly relevant for supervisory decision support where one may prefer conservative escalation when envelopes indicate plausible hazard even if point estimates are small.

The computational cost of constrained learning is moderate. Constrained networks are slightly more expensive than unconstrained ones due to monotone architectures and normalization, but the dominant cost remains simulation and gradient computation [51]. Because constraints reduce solver failures and eliminate time wasted on divergent trajectories, end-to-end training can be more stable and in practice can require fewer restarts. Online deployment uses the trained closures without backpropagation, so runtime cost is comparable to a standard drift-flux simulator, with small overhead for evaluating neural operators.

6 Conclusion

This paper developed a constraint-preserving physics–machine-learning framework for modeling soluble gas-kick transients in drilling annuli by learning closure operators within a conservative drift-flux model that explicitly tracks both free and dissolved methane inventories. The central contribution was a family of monotone and bounded neural closure operators for drift velocity, friction, swelling, solubility capacity, and mass-transfer kinetics, constructed to satisfy key physical inequalities by design [52]. A training formulation combined surface measurement mismatch with weak physics residual penalties and admissibility barriers, while Lipschitz regularization controlled sensitivity and improved robustness under extrapolation. A discrete admissibility analysis showed that, when combined with positivity-preserving transport discretization and implicit relaxation updates for mass transfer, the simulator can preserve nonnegativity of inventories and holdup bounds across time steps, preventing unphysical states that commonly arise in unconstrained learning. Numerical experiments demonstrated that constrained closure learning reduces bias in predicted wellhead pressure and pit gain under closure uncertainty while avoiding solver pathologies in regimes where dissolution masks early free gas and where exsolution accelerates changes later. The operational implication is that, in soluble kick environments, reliability of the model class is determined as much by structural admissibility constraints as by representational flexibility. Constraint-preserving learning provides a pathway to incorporate data-driven closure adaptation without sacrificing physical plausibility, enabling uncertainty-aware envelopes and stable integration into monitoring and supervisory control loops under HPHT conditions [53].

References

[1] N. M. Dinh, *Early kick detection using data-driven bayesian network: Model development and experimental testing*, May 1, 2020.

[2] M. Hornung, "Kick prevention, detection, and control: Planning and training guidelines for drilling deep high-pressure gas wells," *IADC/SPE Drilling Conference*, Feb. 27, 1990. DOI: 10.2118/19990-ms

[3] D. Blakney et al., "Combining state-of-the-art hybrid bit and positive displacement motors saves 863,670 cad over 20 wells in northern alberta, canada," in *SPE Oklahoma City Oil and Gas Symposium*, SPE, Apr. 8, 2019. DOI: 10.2118/195237-ms

[4] A. K. Sleiti, G. Takalkar, M. H. El-Naas, A. R. Hasan, and M. A. Rahman, "Early gas kick detection in vertical wells via transient multiphase flow modelling: A review," *Journal of Natural Gas Science and Engineering*, vol. 80, p. 103 391, 2020.

[5] "Random sample," *Science*, vol. 332, no. 6033, pp. 1018–1018, May 27, 2011. DOI: 10.1126/science.332.6033.1018-a

[6] P. G. Lillis, J. Palacas, and A. Warden, "A precambrian-cambrian oil play in southern utah," *AAPG Bulletin*, vol. 79, no. 6, Jun. 1, 1995.

[7] M. Ikbal, *Evaluasi pemakaian pahat tricone pada pemboran formasi basement (marble, slate) dengan menggunakan metode specific energy dan metode cost per foot pada sumur ''x" lapangan "y" pt. pertamina e.p*, Oct. 26, 2011.

[8] K. Olsvik, M. H. Jondahl, K. R. Toftevåg, R. Kippersund, G. Elseth, and I. Kjøsnes, "Disruptive clamp-on technology tested for mud measurement," in *SPE Norway One Day Seminar*, SPE, May 13, 2019. DOI: 10.2118/195624-ms

[9] R. Rommetveit, "Kick simulator improves well control engineering and planning," *Oil & Gas Journal*, Aug. 22, 1994.

[10] R. P. Coutinho et al., "The case for liquid-assisted gas lift unloading," *SPE Production & Operations*, vol. 33, no. 01, pp. 73–84, Aug. 23, 2017. DOI: 10.2118/187943-pa

[11] J. R. Bowden, "Are you prepared before you start," *SPE Annual Technical Conference and Exhibition*, Sep. 21, 1980. DOI: 10.2118/9253-ms

[12] A. Santos and O. Luiz, "Technology focus: Well integrity and well control," *Journal of Petroleum Technology*, vol. 69, no. 01, pp. 59–59, Jan. 1, 2017. DOI: 10.2118/0117-0059-jpt

[13] E. Saeverhagen, C. Erichsen, A. K. Nesheim, and G. Waldron, "3d rss for 24-in. section sets inclination record on the grane field by introduction of an integrated drilling and surveying bottomhole assembly," in *SPE Annual Technical Conference and Exhibition*, SPE, Sep. 21, 2008. DOI: 10.2118/115330-ms

[14] R. A. Shishavan, C. Hubbell, H. D. Perez, J. D. Hedengren, and D. S. Pixton, "Combined rate of penetration and pressure regulation for drilling optimization by use of high-speed telemetry," *SPE Drilling & Completion*, vol. 30, no. 01, pp. 17–26, Mar. 5, 2015. DOI: 10.2118/170275-pa

[15] F. F. Oliveira, C. H. Sodré, and J. L. G. Marinho, "Flow parameter evaluation during the occurrence of a gas kick in a petroleum drilling using turbulence models: A numerical study," *Brazilian Journal of Petroleum and Gas*, vol. 10, no. 3, pp. 145–159, Oct. 4, 2016. DOI: 10.5419/bjpg2016-0012

[16] N. Nwaka, J. Liu, M. Kunju, and Y. Chen, "Hydrodynamic modeling of gas influx migration in slim hole annuli," *Experimental and Computational Multiphase Flow*, vol. 2, no. 3, pp. 142–150, Nov. 15, 2019. DOI: 10.1007/s42757-019-0038-6

[17] F. Kesuma, *Pengaruh kick off point terhadap perencanaan lintasan pemboran berarah pada sumur w, x, y, z*, Apr. 14, 2016.

[18] K. Manikonda, A. R. Hasan, O. Kaldirim, J. J. Schubert, and M. A. Rahman, "Understanding gas kick behavior in water and oil-based drilling fluids," in *SPE Kuwait oil and gas show and conference*, SPE, 2019, D043S023R001.

[19] T. Lee, K. Lee, K. Sung, and J. Choe, "Well control modeling of oil based mud for various well trajectories," *Journal of the Korean Society of Mineral and Energy Resources Engineers*, vol. 50, no. 4, pp. 482–489, Aug. 1, 2013. DOI: 10.12972/ksmer.2013.50.4.482

[20] X. Chen et al., "Well control for offshore high-pressure/high-temperature highly deviated gas wells drilling: How to determine the kick tolerance?" In *IADC/SPE Asia Pacific Drilling Technology Conference and Exhibition*, SPE, Aug. 27, 2018. DOI: 10.2118/190969-ms

[21] V. Pipicz, L. Benedek, G. Palasthy, T. Barodi, J. Blaho, and S. Joshi, "The fourth horizontal project in the mature algyo field," in *SPE International Thermal Operations and Heavy Oil Symposium and International Horizontal Well Technology Conference*, SPE, Nov. 4, 2002. DOI: 10.2118/78953-ms

[22] P. Oudeman, "Analysis of surface and wellbore hydraulics provides key to efficient blowout control," *SPE Annual Technical Conference and Exhibition*, Oct. 6, 1996. DOI: 10.2118/36485-ms

[23] G. Szekely, E. Peixoto, Z. Czovek, and T. Mezo, "Fast-track development of managed pressure drilling flexible mud return line," in *Offshore Technology Conference*, OTC, May 1, 2017. DOI: 10.4043/27777-ms

[24] P. Qin, A. Andreanov, H. C. Park, and S. Flach, "Interacting ultracold atomic kicked rotors: Loss of dynamical localization," *Scientific reports*, vol. 7, no. 1, pp. 41 139–41 139, Jan. 24, 2017. DOI: 10.1038/srep41139

[25] D. Barnett, "Overview: Well intervention and control (january 2005)," *Journal of Petroleum Technology*, vol. 57, no. 01, pp. 54–54, Jan. 1, 2005. DOI: 10.2118/0105-0054-jpt

[26] D. Dupuis and S. Hancock, "Ad equation between a second generation semi and drilling extended-reach well in tunisia," *IADC/SPE Drilling Conference*, Mar. 4, 2008. DOI: 10.2118/112564-ms

[27] D. Gomes, K. K. Fjelde, K. S. Bjorkevoll, and J. Frøyen, "Gas suspension effects in riser unloading and appropriate modelling approaches," in *Volume 11: Petroleum Technology*, American Society of Mechanical Engineers, Aug. 3, 2020. DOI: 10.1115/omae2020-18049

[28] P. Colombo, "Closed loop controlled electronic carburation system," in *SAE Technical Paper Series*, vol. 1, United States: SAE International, Sep. 28, 2010. DOI: 10.4271/2010-32-0115

[29] K. Manikonda et al., “A mechanistic gas kick model to simulate gas in a riser with water and synthetic-based drilling fluid,” in *Abu Dhabi International Petroleum Exhibition and Conference*, SPE, 2020, D012S116R009.

[30] S. M. Willson, A. S. Nagoo, and M. M. Sharma, “Analysis of potential bridging scenarios during blowout events,” *SPE/IADC Drilling Conference*, pp. 345–363, Mar. 5, 2013. DOI: 10.2118/163438-ms

[31] S. Pentury, *Analisis casing design di sumur high pressure high temperature pada lapangan sp*, Oct. 2, 2019.

[32] A. Hashim and Z. Yasin, “Overview of acid stimulation practices in malaysian oil fields,” in *SPE Asia Pacific Oil and Gas Conference*, SPE, Feb. 8, 1993. DOI: 10.2118/25386-ms

[33] M. Syzdykov and E. Ozkan, “Industry-university collaboration to develop sustainable petroleum engineering program and meet the industry needs in kazakhstan,” in *SPE Annual Technical Conference and Exhibition*, SPE, Sep. 23, 2019. DOI: 10.2118/195903-ms

[34] W. M. Ernata, C. Irawan, Y. R. Sinulingga, B. Irawan, and C. Kalimantan, “Challenge and hydrocarbon potential of sn structure on kutai basin of east kalimantan,” in *SPE Annual Caspian Technical Conference & Exhibition*, SPE, Nov. 1, 2016. DOI: 10.2118/182539-ms

[35] M. Nabaei, A. R. Moazzeni, R. Ashena, and A. Roohi, “Complete loss, blowout and explosion of shallow gas, infelicitous horoscope in middle east,” in *SPE European Health, Safety and Environmental Conference in Oil and Gas Exploration and Production*, SPE, Feb. 22, 2011. DOI: 10.2118/139948-ms

[36] J. A. Onyeji, A. A. Adebayo, T. W. Stafford, O. A. Ekun, H. Onu, and K. K. Nwozor, “Effective real-time pore pressure monitoring using well events: Case study of deepwater west africa - nigeria,” in *SPE Nigeria Annual International Conference and Exhibition*, SPE, Jul. 31, 2017. DOI: 10.2118/189128-ms

[37] S. Noonan, “Spe strong: Strengthening our core: Spe staying strong,” *Journal of Petroleum Technology*, vol. 72, no. 05, pp. 6–7, May 1, 2020. DOI: 10.2118/0520-0006-jpt

[38] A. Fredon and H. M. Cuppen, “Molecular dynamics simulations of energy dissipation and non-thermal diffusion on amorphous solid water.,” *Physical chemistry chemical physics : PCCP*, vol. 20, no. 8, pp. 5569–5577, Feb. 21, 2018. DOI: 10.1039/c7cp06136f

[39] H. M. Gimenez, *A questão agrária na bolívia*, Jul. 10, 2014.

[40] T. M. Bryant, D. S. Grosso, and S. N. Wallace, “Gas-influx detection with mwd technology,” *SPE Drilling Engineering*, vol. 6, no. 04, pp. 273–278, Dec. 1, 1991. DOI: 10.2118/19973-pa

[41] Z. Lippai, Z. Frei, and Z. Haiman, “Prompt shocks in the gas disk around a recoiling supermassive black hole binary,” *The Astrophysical Journal*, vol. 676, no. 1, pp. L5–L8, Mar. 4, 2008. DOI: 10.1086/587034

[42] A. Tallin, P. Paslay, E. P. Cernocky, and M. A. Ratchinsky, “Risk assessment of exploration well designs in the oman ara salt,” in *SPE Annual Technical Conference and Exhibition*, SPE, Oct. 1, 2000. DOI: 10.2118/63130-ms

[43] B. A. Elieff and J. Schubert, “Dual gradient drilling will control shallow hazards in deepwater environments,” in *Volume 7: Offshore Geotechnics; Petroleum Technology*, ASMEDC, Jan. 1, 2009, pp. 509–539. DOI: 10.1115/omae2009-79790

[44] A. Johnson and S. Cooper, “Gas migration velocities during gas kicks in deviated wells,” *SPE Annual Technical Conference and Exhibition*, Oct. 3, 1993. DOI: 10.2118/26331-ms

[45] R. C. Dinata, C. Sarica, and E. Pereyra, “End of tubing eot placement effects on the two-phase flow behavior in horizontal wells: Experimental study,” in *SPE Annual Technical Conference and Exhibition*, SPE, Sep. 26, 2016. DOI: 10.2118/181302-ms

[46] S. Ray and S. D. S. Sinha, *Non-equilibrium dynamics of quantum many body systems: Application to ultracold atomic gases*, May 1, 2019.

[47] C. Hainaut et al., “Return to the origin as a probe of atomic phase coherence,” *Physical review letters*, vol. 118, no. 18, pp. 184 101–, May 5, 2017. DOI: 10.1103/physrevlett.118.184101

[48] B. R. Tulimilli, P. Naik, A. Chakraborty, S. Sawant, and A. Whooley, “Design study of bop shear rams based on validated simulation model and sensitivity studies,” in *Volume 1B: Offshore Technology*, American Society of Mechanical Engineers, Jun. 8, 2014. DOI: 10.1115/omae2014-24305

[49] L. Li et al., “Evaluating wellbore accessibility and productive performance for a long-reach multilateral tight gas well in changbei block,” in *SPE/ICoTA Coiled Tubing & Well Intervention Conference & Exhibition*, SPE, Mar. 24, 2015. DOI: 10.2118/173635-ms

[50] Z. M. Zhi, F. J. Hong, H. Shi, F. Kang, X. Bin, and J. Zhang, “The mechanism of pressure control problem in high h2s/co2 gas wells,” in *International Oil and Gas Conference and Exhibition in China*, SPE, Jun. 8, 2010. DOI: 10.2118/130143-ms

[51] J. Wang, J. Li, G. Liu, M. Li, K. Luo, and G. Zhang, "Development and application of transient gas-liquid two-phase flow model considering sudden density change," *Energy Science & Engineering*, vol. 8, no. 4, pp. 1209–1219, Dec. 12, 2019. DOI: 10.1002/ese3.579

[52] H. Santos, E. Catak, and S. Valluri, "Kick tolerance misconceptions and consequences to well design," *SPE/IADC Drilling Conference and Exhibition*, Mar. 1, 2011. DOI: 10.2118/140113-ms

[53] Y. Dadmohammadi et al., "Integrating human factors into petroleum engineering's curriculum: Essential training for students," in *SPE Annual Technical Conference and Exhibition*, SPE, Oct. 9, 2017. DOI: 10.2118/187241-ms